JOURNAL OF THERMOPHYSICS AND HEAT TRANSFER
Vol. 6, No. 4, Oct.–Dec. 1992

Practical Model for Molecular Contaminant Deposition Kinetics

A. P. M. Glassford*
Lockheed Missiles & Space Company, Sunnyvale, California 94089

A practical model for molecular contaminant deposition kinetics has been developed. The model is based on physically realistic expressions for the monolayer adsorption, multilayer adsorption, nucleation, and bulk condensation processes, but is simple enough to be used in routine engineering spacecraft contamination migration studies. The model was evaluated against deposition and evaporation data measured for a flux of simulated molecular contaminant, tetramethyl tetraphenyl trisiloxane, impinging on an aluminum-coated quartz crystal microbalance (QCM) held at temperatures between 273 K and 303 K. The range of impinging fluxes used permitted both equilibrium adsorption and bulk deposition phenomena to be measured. It was concluded that the model represented the data well, both qualitatively and quantitively, and that the most important data required to support deposition modeling purposes was the evaporation rate of the deposit as a function of deposit mass. Although the model was intended primarily to support practical engineering design analyses, it was found to be capable of modeling the main physical processes involved in molecular deposition and evaporation in a manner consistent with scientifically more rigorous studies.

Nomenclature

C = condensation coefficient
E_{ao}, E_{am} = monolayer, multilayer adsorption energy, cal/mole
f_b = surface area fraction covered by islands of bulk material
f_m = surface area fraction by multilayer adsorption
M = molecular weight of impinging species
m_{ado}, m_{adm} = monolayer, multilayer adsorbed mass, g/cm^2
m_{adt} = total mass adsorbed, $m_{ado} + m_{adm}$, g/cm^2
m_{dep} = total mass adsorbed and condensed, g/cm^2
m_o, m_m = monolayer, multilayer adsorption capacity, g/cm^2
$\dot{m}_{ado}$, $\dot{m}_{adm}$ = monolayer, multilayer adsorption rate, g/cm^{2}s
$\dot{m}_{adt}$ = total adsorption rate, $\dot{m}_{ado} + \dot{m}_{adm}$, g/cm^{2}s
$\dot{m}_b$ = bulk material evaporation rate, g/cm^{2}s
$\dot{m}_{dep}$ = total mass deposition rate, g/cm^{2}s
$\dot{m}_{ed}$ = evaporation rate during net deposition, g/cm^{2}s
$\dot{m}_{ee}$ = evaporation rate with no impinging flux, g/cm^{2}s
$\dot{m}_i$ = impingement rate, g/cm^{2}s
P_v = vapor pressure, dynes/cm^2
R = universal gas constant, cal/mole K
R_s, R_{sc} = supersaturation ratio, critical supersaturation ratio
S_e = effective sticking coefficient, defined by Eq. (6)
S_o, S_m = sticking coefficient on bare surface, adsorbed layers
T_s, T_e = QCM1 surface, effusion cell temperature, K
α_e = evaporation coefficient
τ_{ao}, τ_{am} = monolayer, multilayer infinite temperature residence time, s
τ_o = monolayer residence time, $\tau_{ao} \exp(E_{ao}/RT_s)$, s
τ_m = multilayer residence time, $\tau_{am} \exp(E_{am}/RT_s)$, s

Received April 25, 1991; revision received Sept. 9, 1991; accepted for publication Sept. 10, 1991.
*Senior Staff Engineer, Space Systems Division Org. 62-61, Bldg. 589, 1111 Lockheed Way. Member AIAA.

Introduction

MOLECULAR contaminants can degrade the performance of space systems by changing the optical properties of optical system and thermal control surfaces.[1] Molecular contamination is controlled using modeling codes to predict contamination levels from outgassing, thruster plumes, liquid dumps, and so forth, and adjusting the system design and operation to keep these levels within acceptable limits. Many complex phenomena are involved in the prediction of contamination generation, migration, deposition, and optical effects, and it is costly and technically difficult to develop physically rigorous codes. Consequently, the models currently used in the aerospace industry frequently make use of empirical expressions and approximations. However, future space systems will require greater performance at lower cost, so more rigorous prediction models are needed in order to confidently set design and operational constraints which are adequate but not excessive.

An essential component of a contamination prediction code is the deposition kinetics model, which relates contaminant impingement rate to surface mass deposition rate. A complete deposition model would represent simultaneous transient adsorption and desorption, surface diffusion and nucleation, bulk condensation and evaporation, surface chemical reactions, and the effect of the space environment. Most of the substantial literature on these phenomena has addressed these phenomena separately and has studied low-molecular-weight species and well-characterized surfaces, usually for equilibrium conditions. In contrast, space system surfaces are usually poorly characterized and will already be contaminated to some unknown degree before reaching orbit. The contaminant flux will be a mixture of molecular species, some of which will be high-molecular-weight polymers, whose relative proportions will vary with time, and which may interact with each other and the deposition surface. Finally, the space ultraviolet, electron, proton, and atomic oxygen environments can affect the deposition rate and chemistry of the deposit.[2]

The complexity of the space contamination deposition problem has prevented development of a comprehensive, rigorous model, and most current models are either empirically based or physically based expressions valid for only one deposition regime. This article proposes an engineering deposi-

tion model that is an improvement over current models, because it is capable of representing the main physical deposition phenomena of monolayer adsorption, multilayer adsorption, nucleation, and bulk condensation. Published kinetic models for these phenomena are reviewed, and a simple unified kinetic deposition model is developed. The model was evaluated by assessing its ability to represent measured deposition data in a physically consistent manner. The deposition data used for this evaluation were measured in a series of tests in which the deposition surface was simulated by an isothermal quartz crystal microbalance, and the contaminant flux was simulated by a representative silicone oil.

Deposition Model

This section reviews published kinetic models for the four main physical phenomena involved in surface deposition: monolayer adsorption, multilayer adsorption, nucleation, and bulk condensation. Because the article addresses a practical rather than scientific application, the simplest models are considered rather than the most rigorous. The separate models are then combined into a unified model for deposition kinetics from monolayer adsorption through bulk condensation.

Monolayer Adsorption

The simplest model for monolayer adsorption is due to Langmuir.[3] It assumes that impinging molecules which strike an already-adsorbed molecule will be reflected. Surface diffusion and interactions between molecules are neglected, and the net adsorption rate is expressed as the difference between the gross adsorption rate and the desorption rate. For the case of no dissociation this model can be expressed in mass terms by Eq. (1):

$$\dot{m}_{ado} = \dot{m}_i S_o(1 - m_{ado}/m_o) - m_{ado}/\tau_o \qquad (1)$$

Multilayer Adsorption

Measurements on practical surfaces frequently indicate sorption capacities greater than a nominal completed monolayer. Capacities higher than a nominal monolayer, but with monolayer adsorption energy, can occur if the exposed area of a surface is greater than nominal because of roughness effects. Higher sorption capacities can also be obtained by formation of multiple adsorbed layers on top of a monolayer or by filling of surface pores and imperfections. The Brunauer-Emmett-Teller (BET) multilayer adsorption model[3] extends the Langmuir monolayer model to include adsorption on top of already-adsorbed molecules. The BET model assumes monolayer adsorption energy for the first layer and a lower adsorption energy closer to the latent heat of the adsorbed species for the subsequent layers. The transient form of BET model permits detailed analyses of multilayer sorption rates[4] but is too complex for the present purposes. The character of sorption by porous surfaces depends very strongly on the size of the pores relative to the diameter of the sorbed molecules[5] and is complex to model because pore sizes and sorption energies typically have distributions of values.[6] In general the adsorption energy within the pores will be higher than the monolayer adsorption energy. Because the mechanism responsible for higher sorption capacities is not known in advance for engineering surfaces, this article proposes a simple model for sorption capacities higher than a monolayer, which is insensitive to whether the higher capacity is due to surface roughness, pores, or multilayer adsorption. The surface is assumed to be separated into a monolayer sorption region with sorption energy E_{ao} and area fraction $(1 - f_m)$, and a higher capacity sorption region with sorption energy E_{am} and area fraction f_m. The high-capacity region will be referred to as the multilayer region in accordance with common practice. The total adsorption rate is the sum of the sorption rates given by Eq. (1) for each region:

$$\dot{m}_{adt} = (1 - f_m)\{\dot{m}_i S_o(1 - m_{ado}/m_o) - m_{ado}/\tau_o\} + f_m\{\dot{m}_i S_m(1 - m_{adm}/m_m) - m_{adm}/\tau_m\} \qquad (2)$$

Nucleation

When surface-diffusing adsorbed molecules collide they can form clusters which, under certain conditions, become stable nuclei for bulk condensation. The two major models for determining the conditions for nucleation are the critical cluster model and the kinetic model. The critical cluster model[7,8] states that clusters must be greater than a certain size in order to be thermodynamically stable. If the impinging flux has to be raised above the evaporation rate of the bulk condensed phase to form critical-sized clusters, then a "nucleation barrier" is said to exist. The nucleation barrier is quantified by the supersaturation ratio R_s, defined as the ratio of the impinging flux to the bulk evaporation rate. The critical supersaturation ratio R_{sc} is the value of R_s at the onset of bulk condensation. If there is no nucleation barrier, R_{sc} is unity. The kinetic model[9-13] consists of a set of equations which express the rate of formation of clusters containing various numbers of molecules as the algebraic sum of the rates of collision of single molecules, dissociation of larger clusters, combination of smaller clusters, and so forth. The kinetic model has no inherent nucleation barrier and instead accounts for the apparent barrier as a long time constant between establishment of an impinging flux equal to the evaporation rate and the initiation of bulk condensation.

The critical cluster and kinetic models address only simple interactions between sorbed molecules and are not able to model interactions with real, heterogeneous surfaces. Complex intermolecular and molecular-surface interactions on heterogeneous surfaces can be modeled by more powerful mathematical methods such as the Monte Carlo and other approaches.[14]

Formal inclusion of a nucleation kinetics in the deposition model would increase its complexity and would have practical relevance only if the nucleation barrier were significant. Hence nucleation kinetics has not been included in the deposition model in the first instance, and the issue will be reconsidered if the measured data indicate that a significant nucleation barrier does exist.

Bulk Condensation

After the onset of nucleation the deposit will consist of bulk material islands surrounded by regions covered by sorbed molecules. The islands gain mass by condensation of impinging flux and by capture of surface-diffusing adsorbed molecules and lose mass by bulk evaporation. The area between the islands gains mass by adsorption of impinging molecules and loses mass by desorption and by capture of surface-diffusing adsorbed molecules by the islands. The net deposition rate is given by Eq. (3):

$$\dot{m}_{dep} = f_b(C\dot{m}_i - \dot{m}_b) + (1 - f_b)\dot{m}_{adt} \qquad (3)$$

Surface diffusion effects do not appear explicitly in Eq. (3) because the mass lost by the sorption region by this mechanism is exactly offset by the mass gained by the island region.

Unified Deposition Model

A unified model for deposition kinetics in the monolayer adsorption, multilayer adsorption, and bulk condensation regimes is obtained by substituting Eq. (2) into Eq. (3):

$$\dot{m}_{dep} = \dot{m}_i\{f_b C + (1 - f_b)[(1 - f_m)S_o(1 - m_{ado}/m_o) + f_m S_m(1 - m_{adm}/m_m)]\} - \{f_b\dot{m}_b + (1 - f_b)[(1 - f_m)m_{ado}/\tau_o + f_m m_{adm}/\tau_m]\} \qquad (4)$$

Equation (5) expresses Eq. (4) more compactly in terms of an effective sticking coefficient S_e and an effective evaporation rate $\dot{m}_{ed}$ both of which are functions of the deposit mass m_{dep}

$$\dot{m}_{dep}(m_{dep}) = S_e(m_{dep})\dot{m}_i - \dot{m}_{ed}(m_{dep}) \quad (5)$$

where

$$S_e(m_{dep}) = f_b C + (1 - f_b)[(1 - f_m)S_o(1 - m_{ado}/m_o) + f_m S_m(1 - m_{adm}/m_m)] \quad (6)$$

$$\dot{m}_{ed}(m_{dep}) = f_b\dot{m}_b + (1 - f_b)[(1 - f_m)m_{ado}/\tau_o + f_m m_{adm}/\tau_m] \quad (7)$$

$S_e(m_{dep})$ is the surface-average probability that molecules impinging on a surface partially bare and partially covered by adsorbed and condensed molecules will be compared. $\dot{m}_{ed}(m_{dep})$ is the surface-average rate at which mass leaves the surface during net deposition. The evaporation rate when $\dot{m}_i$ is zero may be different from $\dot{m}_{ed}(m_{dep})$ and is represented by $\dot{m}_{ee}(m_{dep})$. However, both $\dot{m}_{ee}(m_{dep})$ and $\dot{m}_{ed}(m_{dep})$ are expressed parametrically by Eq. (7).

The supersaturation ratio R_s is given by Eq. (8):

$$R_s = \dot{m}_i/\dot{m}_{ed}(m_{dep}) \quad (8)$$

Equations (5)–(8) constitute the mass deposition model proposed by this article.

Experimental Program

In order to use the model, $S_e(m_{dep})$ and $\dot{m}_{ed}(m_{dep})$ must be known, so an experimental program was conducted to determine these quantities. This section describes the experimental approach, apparatus, measurement procedure, and test matrix.

Experimental Approach

The simplest method for characterising deposition and evaporation kinetics experimentally is to measure the deposition rate of a known impinging flux on an isothermal surface as a function of deposit mass, and then interrupt the impinging flux and measure the evaporation rate as a function of deposit mass. The deposition measurement is represented by Eq. (5). The evaporation measurement in the absence of an impinging flux is represented by Eq. (9), which is obtained by writing Eq. (5) with $\dot{m}_i$ equal to zero, and replacing $\dot{m}_{ee}(m_{dep})$ by $\dot{m}_{ed}(m_{dep})$:

$$\dot{m}_{dep}(m_{dep}) = -\dot{m}_{ee}(m_{dep}) \quad (9)$$

The deposition/evaporation test provides two sets of data for determining three unknowns, $S_e(m_{dep})$, $\dot{m}_{ed}(m_{dep})$, and $\dot{m}_{ee}(m_{dep})$. To resolve $S_e(m_{dep})$ and $\dot{m}_{ed}(m_{dep})$ from these data, either another measurement must be made or an assumption must be made about the value of one of the variables. The rigorous approach would be to make another measurement, but to avoid adding complexity to a basically simple test, a reasonable assumption is sought.

Two reasonable assumptions are considered. The first is that $\dot{m}_{ed}(m_{dep})$ is identical to $\dot{m}_{ed}(m_{dep})$. This assumption should be valid if there are no hysteresis or relaxation effects in the deposit, and if the impinging and evaporating fluxes are low enough for their collision probability to be negligible. With this assumption $S_e(m_{dep})$ can be calculated from Eq. (10), which is obtained by substituting $\dot{m}_{ee}(m_{dep})$ for $\dot{m}_{ed}(m_{dep})$ in Eq. (5) and rearranging

$$S_e(m_{dep}) = \{\dot{m}_{dep}(m_{dep}) + \dot{m}_{ee}(m_{dep})\}/\dot{m}_i \quad (10)$$

Published data for sticking[15] and condensation coefficients[16] for the low impingement rates typical of space systems indicate that $S_e(m_{dep})$ may be close to unity to most regimes. A second reasonable assumption is therefore that $S_e(m_{dep})$ is unity for all deposition regimes. With this assumption $\dot{m}_{ed}(m_{dep})$ can be calculated from deposition data using Eq. (11), which is obtained by setting $S_e(m_{dep})$ equal to unity in Eq. (5) and rearranging

$$\dot{m}_{ed}(m_{dep}) = \dot{m}_i - \dot{m}_{dep}(m_{dep}) \quad (11)$$

The experimental approach was thus to perform a series of isothermal deposition and evaporation tests, to analyze the data using each of these assumptions in turn, and to evaluate the reasonableness of the $S_e(m_{dep})$ or $\dot{m}_{ed}(m_{dep})$ data calculated on the basis of these assumptions.

Experimental Apparatus

The experimental apparatus is shown schematically in Fig. 1. Two quartz crystal microbalances (QCM) are arranged with the same view factor to the orifice of an effusion cell containing a molecular flux source. The effusion cell and QCMs are surrounded by liquid nitrogen-cooled shields to ensure that molecular flux reaches the QCM surfaces only by line-of-sight flow from the effusion cell orifice. Shutters permit the molecular flux to each QCM to be interrupted. The apparatus is placed in a glass bell jar evacuated to less than 2×10^{-7} Torr.

The effusion cell is a cylindrical container with a central cylindrical orifice in its detachable top cover. Cell temperature is controlled by balancing electrical resistance heat input against radiative heat loss to the cold walls. The distance between the cell and the QCMs can be adjusted from outside the vacuum chamber by moving the cell support strut. The molecular source material was (1,3,3,5)-tetramethyl (1,1,5,5)-tetraphenyl trisiloxane (TMTPTS), a silicone oil used in diffusion pumps. TMTPTS was selected because it is representative of high-molecular-weight methylphenyl siloxanes, a family of outgassed species commonly encountered in space systems.[17]

The QCMs are QCM Research Mark 9 units, which incorporate two 10-MHz crystals, a platinum resistance thermometer located between the two crystals, and an oscillator/mixer chip. One crystal is used for deposit mass measurement, while the other is used as a reference. The QCM mass sensitivity is 2.26×10^8 Hz/g/cm^2. The crystals had a nominal 3-μm surface finish, overcoated with an aluminum keyhole electrode of about 1000 Å thickness. This crystal style was used solely because of availability. A scanning electron micrograph

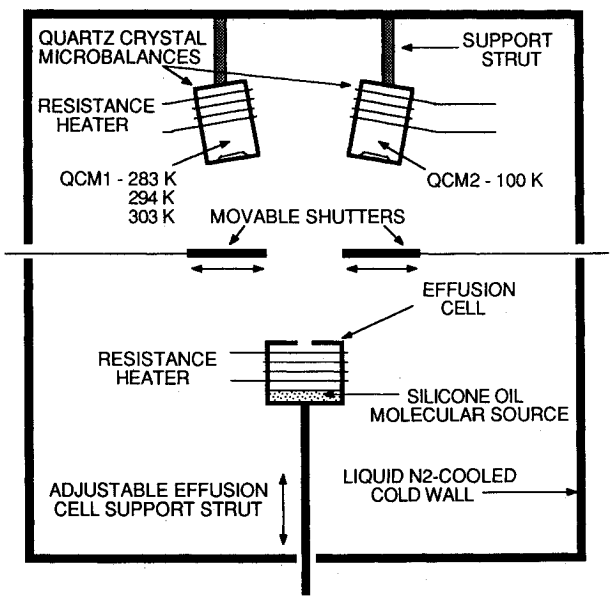

Fig. 1 Schematic of apparatus.

of the crystal surface (Fig. 2) shows that its surface contains a number of porelike imperfections about 1 to 3 μm in diameter. The QCMs are mounted in holders attached by struts to a liquid nitrogen reservoir. The measuring crystal of QCM1 is the test surface. QCM1 is temperature controlled to within ± 0.1 K of a selected test value by balancing electrical resistance heat input to the holders against conductive heat loss along the struts. QCM2 is maintained below 100 K, at which temperature the deposition rate of TMTPTS is effectively equal to the impingement rate. Since both QCMs have the same view factor of the effusion cell orifice, their impingement rates should be the same, so the impingement rate on QCM1 is determined by the deposition rate on QCM2. The equivalence of the QCM view factors was verified in a preliminary test in which both QCMs were cooled below 100 K. The deposition rate indicated by the two QCMs agreed to within $\pm 0.5\%$.

Experimental Procedure

At the start of an experiment the QCM1 measuring crystal was cleaned by heating it to its maximum operating temperature of 400 K. The effectiveness of this cleaning method was validated in two preliminary tests. First, it was found that after repeated cycles of heating and recooling, the frequency was reproducible to about ± 2 Hz, or about ± 1 Å, which is less than the resolution of the test data and hence negligible. Second, the effectiveness of removing TMTPTS from the crystal by heating was compared to solvent cleaning by analyzing the surface using SIMS; less silicon was found on the surface following a heating cycle than following solvent cleaning. It was concluded from these two observations that cleaning by heating to 400 K in vacuum was as effective as standard solvent cleaning and was adequate for the present purposes.

Following the cleaning cycle, the QCM1 temperature was adjusted to a selected test value. The desired impingement rate was obtained by raising the effusion cell temperature to a preselected value, monitoring the deposition rate on QCM2, and adjusting the distance between the cell and the QCMs. The QCM1 shutter was then opened, and the frequency of QCM1 was recorded as a function of time. In tests at relatively low impingement rates, the deposition rate initially decreased slowly, but then fell increasingly rapidly to zero as an equilibrium adsorbed layer was formed on the crystal. These tests were terminated when adsorption equilibrium had been established. In tests at relatively high impingement rates, the deposition rate remained finite as deposition passed from the adsorption regime into the bulk condensation regime. These tests were terminated when the deposit mass exceeded about 2×10^{-6} g/cm^2, at which point deposition had proceeded far enough into the bulk condensation regime for the rate to become essentially constant.

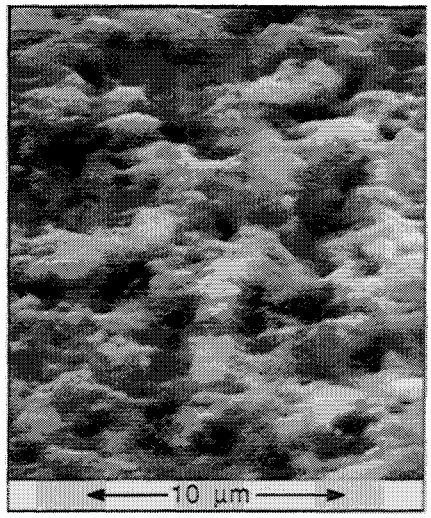

Fig. 2 Scanning electron micrograph of the QCM crystal.

After the deposition test had been terminated by closing the shutters, the frequency of QCM1 was recorded as a function of time as the deposit evaporated. The evaporation test was terminated when the evaporation rate became too small to measure ($<10^{-8}$ g/cm^{2}h).

In general the QCM frequency at the end of an evaporation test did not return to the initial clean frequency before deposition. The differences were as much as ± 4 Hz for some tests, which corresponds to an uncertainty in the mass deposited of about $\pm 2 \times 10^{-8}$ g/cm^2. Since the differences were random throughout the test program, they are attributed to QCM frequency drift.

Test Matrix

Table 1 gives the deposition/evaporation tests parameters. The letter A or B in Table 1 indicates whether a deposition test resulted in the formation of an equilibrium adsorbed layer or continued into the bulk condensation regime, respectively.

At a given QCM1 temperature, the impingement rate was varied between tests by holding the effusion cell temperature constant and changing the distance between the effusion cell and the QCMs. Because deposition kinetics depend strongly on surface temperature, a different range of impingement rates had to be used at each QCM1 temperature in order to cover both the equilibrium adsorption and bulk condensation regimes. Appropriate ranges of impingement rate were obtained by using different effusion cell temperatures for each QCM1 temperature.

Measured Data

Deposition Data

Figures 3, 4, and 5 show deposition rate as a function of deposit mass at 303 K, 294 K, and 283 K, respectively, for various values of impingement rate. For tests which produced bulk deposits, the deposition rate decreases with time in the

Table 1 Deposition/evaporation test matrix

T_s, K	$\dot{m}_i$, g/cm^{2}s	T_e, K	Test type[a]	R_s
303	8.70×10^{-9}	373	B	6.1
303	5.04×10^{-9}	373	B	3.55
303	2.29×10^{-9}	373	B	1.61
303	1.86×10^{-9}	373	B	1.31
303	1.57×10^{-9}	373	B	1.11
303	1.44×10^{-9}	373	A	1.01
303	1.32×10^{-9}	373	A	0.93
303	8.03×10^{-10}	373	A	0.57
294	1.81×10^{-9}	360	B	5.66
294	1.40×10^{-9}	360	B	4.37
294	1.15×10^{-9}	360	B	3.60
294	5.88×10^{-10}	360	B	1.84
294	4.88×10^{-10}	360	B	1.53
294	4.13×10^{-10}	360	B	1.29
294	3.64×10^{-10}	360	B	1.14
294	2.68×10^{-10}	360	A	0.84
283	1.09×10^{-9}	373	B	24.2
283	7.89×10^{-10}	373	B	17.5
283	6.13×10^{-10}	373	B	13.6
283	1.29×10^{-10}	343	B	2.90
283	8.68×10^{-11}	343	B	1.92
283	7.55×10^{-11}	343	B	1.67
283	6.22×10^{-11}	343	B	1.38
283	5.87×10^{-11}	343	B	1.30
283	5.41×10^{-11}	343	B	1.20
283	4.96×10^{-11}	343	A	1.10
283	3.92×10^{-11}	343	A	0.87
283	3.03×10^{-11}	343	A	0.67
283	2.36×10^{-11}	343	A	0.52
273	1.03×10^{-11}	343	B	2.06
273	4.64×10^{-12}	343	A	0.93

[a]A, test produced adsorption equilibrium; B, test produced bulk deposition.

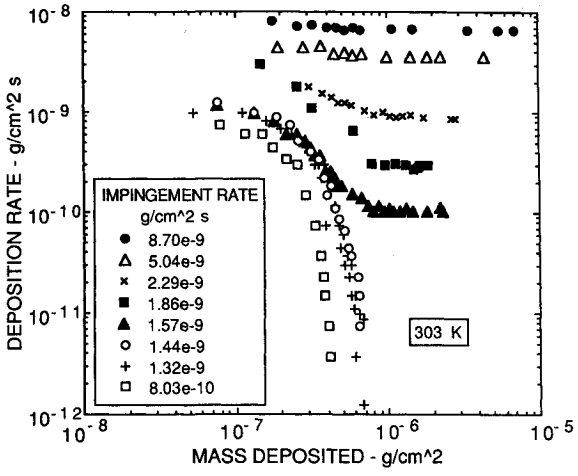

Fig. 3 Deposition rate vs mass deposited, 303 K surface.

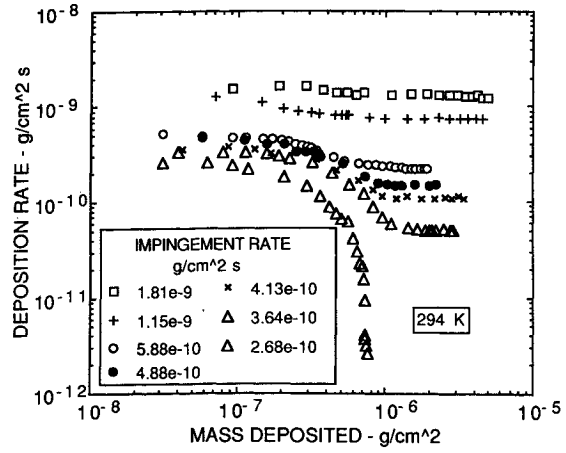

Fig. 4 Deposition rate vs mass deposited, 294 K surface.

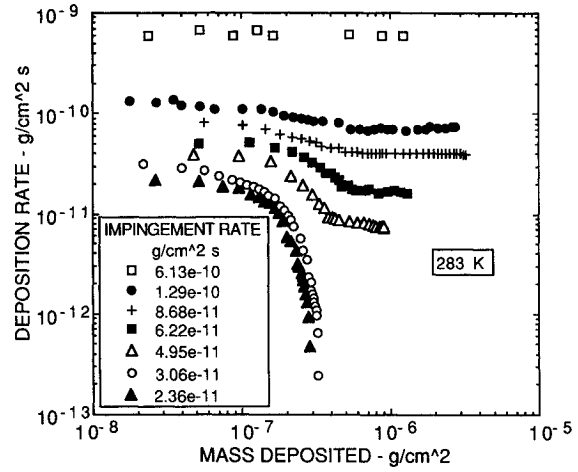

Fig. 5 Deposition rate vs mass deposited, 283 K surface.

deposit mass range up to 80×10^{-8} g/cm^2, and then becomes essentially constant in the bulk deposit regime above about 100×10^{-8} g/cm^2. For tests which produced adsorption equilibrium, the deposition rate decreases with time until equilibrium is reached in the deposit mass range of about 35 to 80 $\times 10^{-8}$ g/cm^2. The equilibrium deposit mass is a function of impingement rate. The specific gravity of TMTPTS is 1.07 and its mean molecular diameter is about 10 Å, so a nominal monolayer corresponds to a deposit mass of about 10×10^{-8} g/cm^2. The deposition data therefore clearly show sorption capacity well in excess of a nominal monolayer.

Evaporation Data

Figure 6 shows deposit mass as a function of time for evaporation at 303 K. Within the sensitivity of the measurements, the evaporation rate vs time characteristics are the same for all tests, regardless of the original deposition rate or the deposit mass when evaporation was initiated. In the bulk regime the characteristic has a relatively constant slope, implying a constant evaporation rate. The evaporation rate decreases steadily through the sorbed deposit mass range below 80×10^{-8} g/cm^2, and then undergoes a marked further decrease as the deposit mass falls below 10×10^{-8} g/cm^2. The 283 K and 294 K test data are qualitatively similar to the 303 K data. This behavior indicates that the residence time and hence sorption energy are lower in the sorbed deposit mass range above the monolayer capacity of 10×10^{-8} g/cm^2 than in the monolayer. This relationship between sorption energies above and below the monolayer is more consistent with the multilayer adsorption model than either the surface roughness or porous surface effects model. In this article, sorption capacities in excess of a monolayer are therefore assumed to be due to multilayer adsorption for the combination of contaminant species and QCM surface studied.

Figures 7, 8, and 9 show evaporation rate as a function of deposit mass at 303 K, 294 K, and 283 K, respectively. At a given temperature the evaporation rate for all tests are essentially coincident, so data from a lesser number of representative tests are shown to minimize clutter. The transition from a constant evaporation rate in the bulk regime to a decreasing evaporation (i.e., desorption) rate in the multilayer sorption regime is clearly evident.

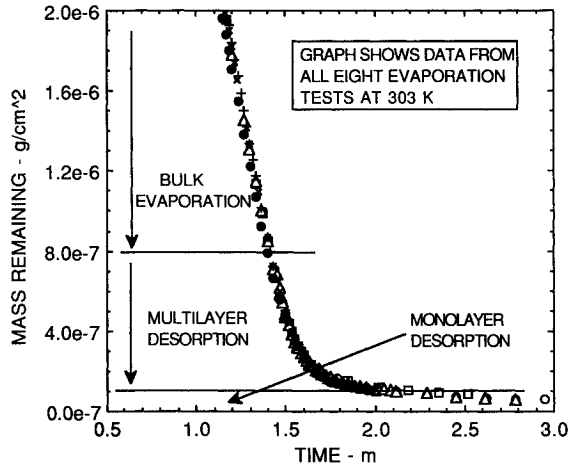

Fig. 6 Mass remaining during evaporation vs time, 303 K surface.

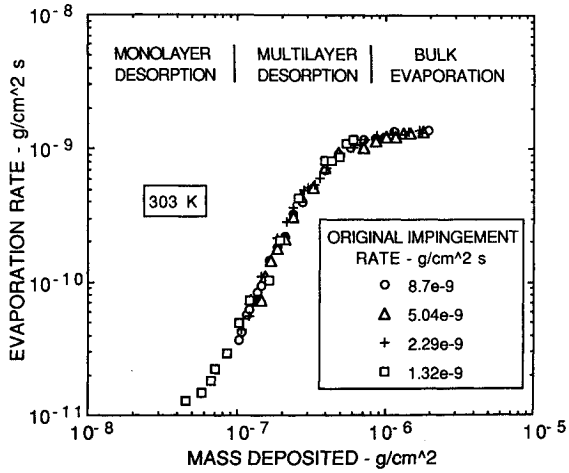

Fig. 7 Evaporation rate vs mass deposited, 303 K surface.

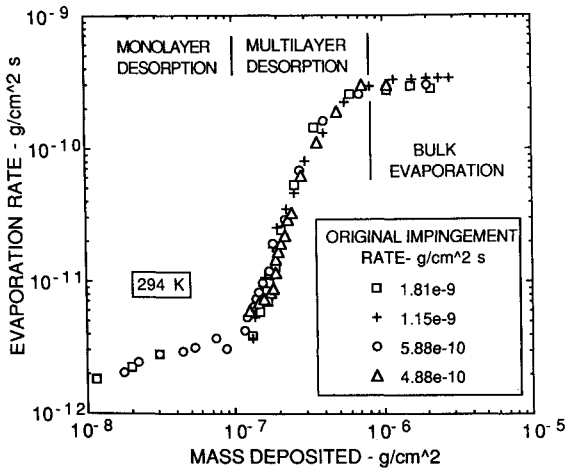

Fig. 8 Evaporation rate vs mass deposited, 294 K surface.

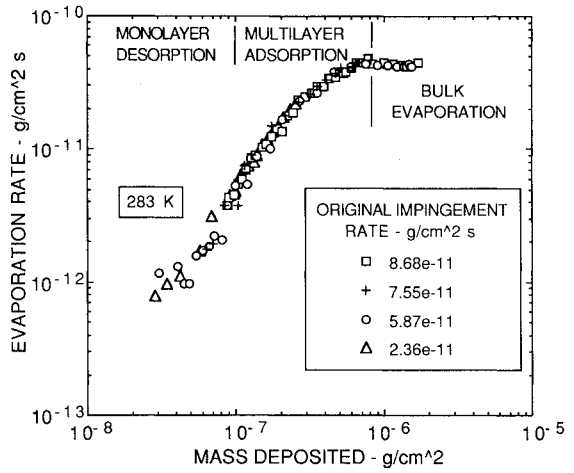

Fig. 9 Evaporation rate vs mass deposited, 283 K surface.

Nucleation Data

Table 1 gives R_s calculated using Eq. (8) and assuming $\dot{m}_{ed}$ to be the value of $\dot{m}_{ee}(m_{dep})$ for the bulk evaporation portion of Figs. 7–9. The lowest R_s value for which bulk condensation was obtained was 1.11 (303 K; 1.57×10^{-9} g/cm²s), while the highest value for which bulk condensation was not obtained was also 1.10 (283 K; 4.96×10^{-10} g/cm²s). R_{sc} must therefore be on the order of 1.10, which is close enough to unity to conclude that there is no significant nucleation barrier.

Discussion

The deposition data are analyzed in two ways. First, it is assumed that $\dot{m}_{ee}(m_{dep})$ is identical to $\dot{m}_{ed}(m_{dep})$ and $S_e(m_{dep})$ is calculated using Eq. (10). Second, it is assumed that $S_e(m_{dep})$ is unity and $\dot{m}_{ed}(m_{dep})$ is calculated using Eq. (11). The reasonableness of these two approaches is evaluated by assessing the physical consistency of the behavior of the calculated $S_e(m_{dep})$ and $\dot{m}_{ed}(m_{dep})$ data, respectively. The section begins with a discussion of the evaporation rate data $\dot{m}_{ee}(m_{dep})$, since its behavior affects both approaches.

Evaporation Rate

The data of Figs. 5–7 show that, within the parameter range of these experiments, the evaporation rate in the absence of an impinging flux, $\dot{m}_{ee}(m_{dep})$, depends only on surface temperature and mass deposited and is independent of the original impingement and deposition rates. This is the most significant conclusion to be drawn from the test program. It shows that $\dot{m}_{ee}(m_{dep})$ is a property of a contaminant/surface system, and that it can be determined from a single evaporation test at each temperature. The behavior of the $\dot{m}_{ee}(m_{dep})$ data can be compared with the physical models presented earlier.

During bulk deposition the deposit consists of islands of bulk material with adsorbed molecules between the islands. When the impinging flux is interrupted, the adsorbed molecular population will be rapidly depleted by desorption and by capture by the islands, so during evaporation the desorption terms in Eq. (7) will be negligible, and $\dot{m}_{ee}(m_{dep})$ will be equal to $f_b\dot{m}_b$. Since $\dot{m}_{ee}(m_{dep})$ is constant in the bulk regime (Figs. 5–7), $f_b\dot{m}_b$ must also be constant. The evaporation rate of bulk condensate is given by the Langmuir equation, Eq. (12):

$$\dot{m}_b = \alpha_e P_v (M/2\pi RT_s)^{1/2} \tag{12}$$

Published data[18] suggest that α_e should be close to unity for the low evaporation rates used in the current tests, so $\dot{m}_b$ will be constant. If both $\dot{m}_b$ and $f_b\dot{m}_b$ are constant, f_b must be constant, and the islands must lose mass at constant base area. Table 2 gives f_b estimated by dividing $\dot{m}_{ee}(m_{dep})$ for the bulk evaporation portion of Figs. 5–7 by $\dot{m}_b$ calculated from Eq. (12) using published vapor pressure data.[19–21] The f_b values are about one quarter to one half the theoretical maximum value of $\pi/4$ for square-packed identical round islands and are consistent with photographic data,[22] as well as values calculated for TMTPTS deposited on a similar QCM.[23] The increase of f_b with temperature may be due to higher mobility and hence higher degree of relaxation of the surface or to lower surface tension and hence lower contact angle.

Because both $\dot{m}_b$ and $\dot{m}_{ee}(m_{dep})$ are independent of the original deposition rate, f_b must also be independent of deposition rate. A possible explanation is that during deposition, adsorbed molecules migrate over the QCM surface and nucleate at surface defects. If the surface mobility of condensed molecules is high relative to the deposition rate, the deposit will have time to adjust completely to the surface topology. The island number density will then be determined only by the number of surface defects and will be the same for all tests.

The deposit mass evaporates from about 80×10^{-8} g/cm² down to 10×10^{-8} g/cm² by multilayer desorption. In this regime the desorption rate is given by Eq. (13) below, which is obtained by setting f_b equal to zero in Eq. (7):

$$\dot{m}_{ee}(m_{dep}) = (1 - f_m)m_{ado}/\tau_o + f_m m_{adm}/\tau_m \tag{13}$$

The adsorption energy and hence residence time should be significantly higher in the monolayer than in the multilayer regime, so the monolayer term in Eq. (13) should be small by comparison with the multilayer term, and $\dot{m}_{ee}(m_{dep})$ should be approximately equal to $f_m m_{adm}/\tau_m$. If f_m and E_{am} are reasonably constant and if the multilayer adsorption energy is also constant $\dot{m}_{ee}(m_{dep})$ should be a linear function of m_{adm} with slope equal to f_m/τ_m. When Figs. 5–7 are replotted on linear axes, this linearity is evident. When the slopes of the linear portions are plotted in the form log (τ_m/f_m) vs $(1/T_s)$, a straight line is obtained with a best-fit slope of 14,400 K, implying a multilayer adsorption energy of 28.5 kcal/mol. This is slightly higher than the published latent heat for TMTPTS of 25.5 kcal/mol[19–21] and is hence consistent with published data for multilayer sorption energies,[5] as well as the assumptions of the BET model.

Table 2 Bulk deposit coverage factor

T_s, K	$\dot{m}_{ee}$, g/cm²s	$\dot{m}_b$, g/cm²s[a]	f_b
303	1.42×10^{-9}	3.54×10^{-9}	0.40
294	3.20×10^{-10}	9.33×10^{-10}	0.34
283	4.50×10^{-11}	1.64×10^{-10}	0.27
273	5.00×10^{-12}	2.98×10^{-11}	0.17

[a]Based on averaged P_v data from Refs. 19–21.

Figures 5–7 all show that the dependence of $\dot{m}_{ee}$ on m_{dep} changes in the region below about 10×10^{-8} g/cm^2 to a characteristic with a smaller slope. This is consistent with a change in the evaporation process from multilayer desorption to monolayer desorption, with a corresponding increase in desorption energy and hence residence time. However, because of the lower desorption rates and experimental time constraints, fewer data were obtained in this regime, so monolayer adsorption energies could not be reliably deduced.

Effective Sticking Coefficient

For the multilayer adsorption and bulk deposition regimes, $S_e(m_{dep})$ was calculated for each deposition test by inserting the $\dot{m}_{dep}(m_{dep})$ and $\dot{m}_i$ data into Eq. (10), along with the value of $\dot{m}_{ee}(m_{dep})$ for the same value of m_{dep}. The $\dot{m}_{eep}(m_{dep})$ and $\dot{m}_{ee}(m_{dep})$ data were measured, in general, at different values of m_{dep}, so the $\dot{m}_{ee}(m_{dep})$ data had to be interpolated in order to complete this calculation. To facilitate the interpolation, the $\dot{m}_{ee}(m_{dep})$ data for each temperature were curve-fitted using an empirical expression of the following form:

$$\dot{m}_{ee}(m_{dep}) = (1/(1/(am_{dep}^b)^c + 1/d^c))^{1/c} \qquad (14)$$

The values used for the constants a, b, c, and d were 1.28×10^5, 2.2, 1.4, and 1.42×10^{-9} at 303 K; 6×10^{12}, 3.3, 1.0, and 3.2×10^{-10} at 294 K; and 18, 1.8, 1.5, and 4.5×10^{-11} and 283 K.

The calculated values of $S_e(m_{dep})$ for 303 K are plotted vs deposit mass in Fig. 10. For all impingement rates, $S_e(m_{dep})$ is close to unity in the monolayer adsorption region, passes through a more or less strongly defined minimum in the multilayer region, and is asymptotic to a value of about 1.0 in the bulk regime. The 294 K and 283 K data behave in a similar manner to the 303 K data, with bulk deposit asymptotic values of 0.97 and 1.08, respectively.

The slight difference in the bulk regime value of $S_e(m_{dep})$ between temperatures is not systematic and is probably caused by random misalignment of the effusion cell orifice axis with respect to the two QCMs when the cell was removed and replaced between test series for refilling with silicone oil. Misalignment would cause the flux on QCM1 to differ from the flux on QCM2 by a constant factor for all tests at each temperature, which would introduce a constant error in the assumed value of $\dot{m}_i$, and hence in the value of $S_e(m_{dep})$ calculated from Eq. (10). It is therefore concluded that $S_e(m_{dep})$ is unity in the bulk regime within the accuracy of these measurements.

Equation (6) indicates that for $S_e(m_{dep})$ to be unity for coverage factors in the range of 0.2 to 0.4 (Table 2), the terms C, $S_o(1 - m_{ado}/m_o)$, and $S_m(1 - m_{adm}/m_m)$ must also be unity. For the low impingement rates typical of orbital contamination rates, C should be close to unity,[16] and the discussion of the next paragraph concludes that S_o is also unity. S_m should lie somewhere between S_o and C and therefore should also be close to unity. In order for the terms $(1 - m_{ado}/m_o)$ and $(1 - m_{adm}/m_m)$ to be unity, the monolayer and multilayer coverages, m_{ado}/m_o and m_{adm}/m_m, must be negligibly small during bulk condensation. However, these coverages must be very high before nucleation can occur, so for $S_e(m_{dep})$ to be unity after the initiation of bulk condensation, a mechanism must appear which removes molecules from the area between the bulk deposit islands as soon as they are adsorbed. This mechanism is believed to be capture of surface-diffusing adsorbed molecules by the islands.

In the multilayer regime $S_e(m_{dep})$ is unity at very high impingement rates, but passes through increasingly pronounced minima with decreasing impingement rate. However, for the impingement rates which produced sorption equilibrium, $S_e(m_{dep})$ rises from the minimum back to unity as equilibrium is approached. Thus in this region the calculated value of $S_e(m_{dep})$ at a given value of m_{dep} can both decrease or increase with impingement rate. It is difficult to construct a simple physical explanation for this behavior, and it is believed that it occurs only because the substitution of $\dot{m}_{ee}(m_{dep})$ for $\dot{m}_{ed}(m_{dep})$ used in Eq. (10) to calculate $S_e(m_{dep})$ is not valid for all conditions in the multilayer regime. It is significant that, given enough time, $S_e(m_{dep})$ does become unity in this regime, which suggests that a relaxation mechanism may be occurring.

Few $\dot{m}_{ee}(m_{dep})$ data were obtained for the monolayer regime, and Eq. (10) could not be used with confidence, so $S_e(m_{dep})$ was determined by back-extrapolation. When the data of Figs. 3–5 are replotted on an expanded scale, it is found that, for all tests, linear back-extrapolation of the $\dot{m}_{dep}(m_{dep})$ data to zero mass gives $\dot{m}_{dep}(0)$ values within ±3% of $\dot{m}_i$. It was concluded that within the accuracy of these measurements $S_e(0)$ and hence S_o are effectively unity.

Evaporation Rate During Net Deposition

In the second data analysis approach it was assumed that $S_e(m_{dep})$ is unity in all regimes, and $\dot{m}_{ed}(m_{dep})$ was calculated using Eq. (11). It was found that for all deposition tests at all three temperatures, the calculated $\dot{m}_{ed}(m_{dep})$ data are equal to the measured $\dot{m}_{ee}(m_{dep})$ data in the bulk regime, but are greater than or equal to $\dot{m}_{ee}(m_{dep})$ in the multilayer regime. The difference in the multilayer regime is greatest for the lowest impingement rates and decreases to zero at high impingement rates. The difference is also zero at multilayer sorption equilibrium.

Figure 11 shows calculated $\dot{m}_{ed}(m_{dep})$ and measured $\dot{m}_{ee}(m_{dep})$ data for the 303 K tests with impingement rates of 1.32 ×

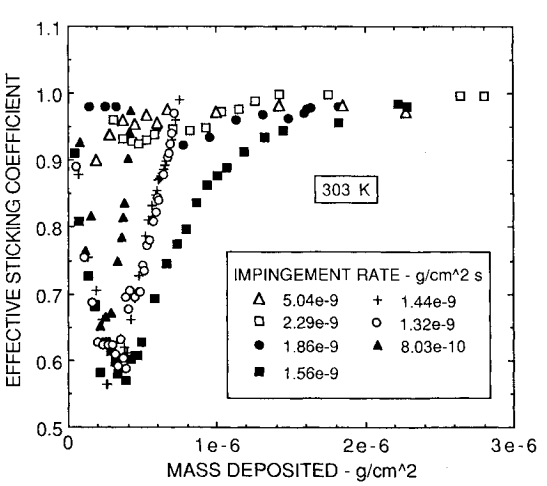

Fig. 10 Effective sticking coefficient vs mass deposited, 303 K surface.

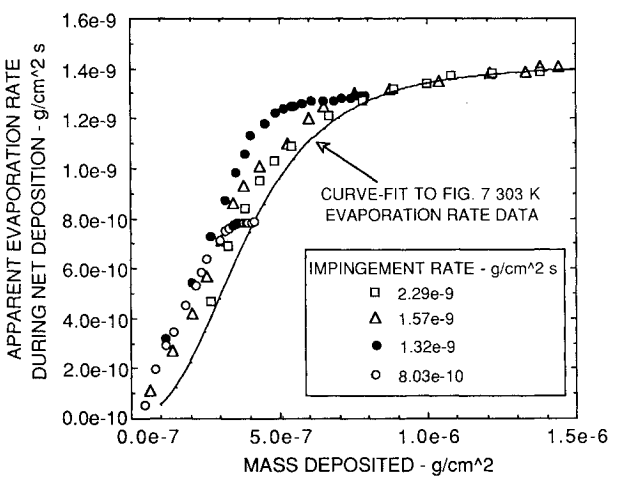

Fig. 11 Comparison of evaporation rate from 303 K surface measured during evaporation test with apparent evaporation rate during deposition calculated from deposition data.

10^{-9} and 8.03×10^{-10} g/cm²s, which produce sorption equilibrium, 1.57×10^{-9} and 2.29×10^{-9} g/cm²s, which produced a bulk deposit. To minimize clutter the $\dot{m}_{ee}(m_{dep})$ data are represented by a curve fit [(Eq. (14)] to the data of Fig. 7. During the initial stages of multilayer adsorption, $\dot{m}_{ed}(m_{dep})$ for the two sorption equilibrium tests follow a characteristic displaced from the $\dot{m}_{ee}(m_{dep})$ characteristic towards lower deposit masses. As sorption equilibrium is approached, $\dot{m}_{ed}(m_{dep})$ tends toward and eventually joins the $\dot{m}_{ee}(m_{dep})$ characteristic. In the multilayer region the two bulk deposit $\dot{m}_{ed}(m_{dep})$ characteristics lie slightly below the sorption equilibrium $\dot{m}_{ed}(m_{dep})$ characteristics, but are still higher than $\dot{m}_{ee}(m_{dep})$. Once the bulk regime is reached $m_{ed}(m_{dep})$ becomes equal to $\dot{m}_{ee}(m_{dep})$. The 294 K and 283 K data behave in a manner similar to the 303 K data.

The relationship between the $\dot{m}_{ed}(m_{dep})$ and $\dot{m}_{ee}(m_{dep})$ characteristics indicate that in the multilayer adsorption regime a given evaporation rate corresponds to the same or lower deposit mass during deposition than during evaporation, and that the difference disappears as equilibrium is reached. This behavior is characteristic of a relaxation process, which may occur in the following manner. The impinging flux is uniform so molecules will initially be adsorbed more or less uniformly over the QCM surface. They will then adjust to the heterogeneous surface by diffusing across it and filling higher energy surface defects. If this relaxation process takes a significant time to complete, the instantaneous desorption rate for a given deposit mass will be higher than at equilibrium, because a larger fraction of the adsorbed molecules will still reside in lower energy sites. When relaxation is complete the desorption rate will have a value consistent with completely filled high energy sites, which is, in fact, the value measured during the evaporation test, $\dot{m}_{ee}(m_{dep})$. The difference between $\dot{m}_{ed}(m_{dep})$ and $\dot{m}_{ee}(m_{dep})$ will be less at the higher impingement rates, because the consequent higher population of adsorbed molecules will shorten the relaxation time. This interpretation of the data is qualitatively consistent with published data, so it is concluded that the assumption that $S_e(m_{dep})$ is always unity is more reasonable than the assumption that $\dot{m}_{ed}(m_{dep})$ is always equal to $\dot{m}_{ee}(m_{dep})$.

Conclusions

A kinetic model has been developed for contaminant flux deposition in the monolayer adsorption, multilayer adsorption, and bulk condensation regimes. The measured deposition data show significantly different behavior in these regimes, confirming the need for a model capable of reflecting these differences. Although both the model and measurement technique are intentionally simple, they lead to qualitative and quantitative conclusions about the physical processes involved in deposition kinetics which are generally consistent with more rigorous published scientific studies.

The major conclusion is that the most important type of experimental data needed to support modeling is evaporation rate as a function of mass deposited. It has been industry practice to characterize deposition kinetics by QCM net deposition rate measurements, principally because these are the primary data generated by standard materials characterisation tests, thermal-vacuum tests, and on-orbit spacecraft environmental measurements. However, deposition rate is a system rather than material property, since impingement rate is a function of system parameters such as view factor from source to condensing surface. On the other hand, the data clearly show that evaporation rate is an impingement-independent property of the contaminant/surface system.

Although the deposition/evaporation test is more complex and provides more information than deposition tests normally used in the industry, it still does not provide enough data to permit all properties to be determined explicitly, and an assumption must be made about either the value of $S_e(m_{dep})$ or the equivalence of $\dot{m}_{ed}(m_{dep})$ and $\dot{m}_{ee}(m_{dep})$ in order to complete the data analysis. The assumption that $S_e(m_{dep})$ is unity in all regimes leads to physically reasonable conclusions. The assumption that $\dot{m}_{ed}(m_{dep})$ is the same as $\dot{m}_{ee}(m_{dep})$ seems valid in most regimes, but there appears to be a relaxation process during multilayer adsorption that causes $\dot{m}_{ed}(m_{dep})$ to be greater than $\dot{m}_{ee}(m_{dep})$ until equilibrium is reached. It is noted that neither of these assumptions is necessarily scientifically correct, since it is possible that for nonequilibrium conditions in the multilayer regime, $S_e(m_{dep})$ may be less than unity, the $\dot{m}_{ed}(m_{dep})$ may also be greater than $\dot{m}_{ee}(m_{dep})$. However, this situation does not lead to a practical methodology for interpreting the deposition/evaporation test data.

Since $\dot{m}_{ed}(m_{dep})$ may be greater than $\dot{m}_{ee}(m_{dep})$, the assumption that $\dot{m}_{ed}(m_{dep})$ is the same as $\dot{m}_{ee}(m_{dep})$ may lead to an overestimate of net deposition rate. The degree of overestimation will be negligibly small for large impingements rates, but will become increasingly significant as the impingement rate decreases.

The model predicts areal mass deposition rate and represents deposit morphology only by the parameter f_b. To model morphology surface diffusion and nucleation kinetics terms would have to be introduced into Eqs. (2) and (3), which would complicate the algebra and would introduce additional parameters which would have to be measured experimentally. Nevertheless, the optical effects of surface contaminants are strongly dependent upon morphology, and extension of the model to predict deposit morphology would be of great value to the modeling community.

The above conclusions apply only to a particular combination of contaminant species, deposition surface, and environment, so the model should be reevaluated for other materials, environments, and test parameters. Many engineering surfaces are smooth and will have lower multilayer adsorption capacity than the unpolished QCM, so relaxation processes may be less apparent. Space system contamination requirements typically call for deposit masses not to exceed about 10^{-6} to 10^{-5} g/cm² over a period of several years, which corresponds to average deposition rates several orders of magnitude lower than the rates considered here. Lower deposition rates over longer periods of time may permit long time constant processes not apparent in short term laboratory tests to assume greater significance. In practice the impinging flux generally contains more than one molecular species, whose interactions may affect deposition kinetics. The space ultraviolet radiation and atomic oxygen environments will all have a major effect on deposition, particularly in the adsorption regime.

Acknowledgments

The author acknowledges the contributions of three colleagues at the Lockheed Missiles & Space Company. C.-K. Liu performed many of the deposition tests. Richard A. Osiecki and Jeffrey W. Garrett generated a computer code for processing the QCM data.

References

[1]Chen, A. T., Abe, N. D., Mullen, C. R., and Gilbert, C. C., "Contamination Sensitivity and Control of Optical Sensors," *Optical System Contamination: Effects, Measurement, and Control,* Vol. 777, Society of Photo-Optical Instrumentation Engineers, Orlando, FL, May 19–22, 1987, pp. 97–126.

[2]Stewart, T. B., Arnold, G. S., Hall, D. F., Marvin, D. C., Hwang, W. C., Young Owl, R. C., and Marten, H. D., "Photochemical Spacecraft Self-Contamination—Laboratory Results and Systems Impact," *Journal of Spacecraft,* Vol. 26, No. 5, 1989, 358–367.

[3]de Boer, J. H., "The Quantity S: Unimolecular and Multimolecular Adsorption," *The Dynamical Nature of Adsorption.* Clarendon Press, Oxford, 1953, Chap. V, pp. 54–89.

[4]Fong, M. C., Liu, C.-K., and Glassford, A. P. M., "A Transient Multilayer Adsorption Analysis," *Proceedings of an International Symposium on Spacecraft Materials in the Space Environment,* Centre National d'Etudes Spatiales, European Space Agency, and Centre

d'Etudes & de Recherches de Toulouse, Toulouse, France, June 1982, ESA SP-178, pp. 71–80.

[5]Gregg, S. J., and Sing, K. S. W., *Adsorption, Surface Area, and Porosity*, Academic Press, New York, 1967.

[6]Dayton, B. B., "Outgassing Rate of Contaminated Metal Surfaces," *1961 Eighth National Symposium on Vacuum Technology Transactions,* Pergamon Press, New York, 1962, pp. 42–57.

[7]Bentley, P. D., and Hands, B. A. "The Condensation of Atmospheric Gases on Cold Surfaces," *Proceedings of the Royal Society of London,* Vol. A359, 1978, pp. 319–343.

[8]Sigsbee, R. A., "Vapor To Condensed-Phase Heterogeneous Nucleation," *Nucleation,* edited by A. C. Zettlemoyer, Marcel Dekker, New York, 1969, pp. 151–224.

[9]Zinsmeister, G., "A Contribution to Frenkel's Theory of Condensation," *Vacuum,* Vol. 16, 1966, pp. 529–535.

[10]Zinsmeister, G., "Theory of Thin Film Condensation. Part B: Solution of the Simplified Condensation Equation," *Thin Solid Films,* Vol. 2, 1968, pp. 497–507.

[11]Zinsmeister, G., "Theory of Thin Film Condensation. Part C: Aggregate Size Distribution in Island Films," *Thin Solid Films,* Vol. 4, 1969, pp. 363–386.

[12]Zinsmeister, G., "Zur Kinetik des Kondensationsvorganges," *Kristall und Technik,* Vol. 4, Sec. 6.2, 1970, pp. 207–251.

[13]Zinsmeister, G., "Theory of Thin Film Condensation. Part D: Influence of a Variable Collision Factor," *Thin Solid Films,* Vol. 7, 1971, pp. 51–75.

[14]Abraham, F. F., "Statistical Surface Physics: A Perspective Via Computer Simulation of Microclusters, Interfaces, and Simple Films," *Report on Progress in Physics,* Vol. 45, 1982, pp. 1113–1161.

[15]Langmuir, I., "Monolayers on Solids," *Journal of Chemical Society,* 1940, pp. 511–543.

[16]Hirth, J. R., and Pound, G. M., "Coefficients of Evaporation and Condensation," *Journal of Chemical Physics,* Vol. 64, May 1960, pp. 619–626.

[17]Colony, J. A., "The Identification of Trends in Outgassing Technology," *Proceedings of the 11th Space Simulation Conference,* NASA CP-2150, NASA Scientific and Technical Information Office, Lyndon B. Johnson Space Center, Houston, TX, 1980, pp. 280–290.

[18]Davy, J. G., and Somorjai, G. A., "Studies of the Vaporization Mechanism of Ice Single Crystals," *Journal of Chemical Physics,* Vol. 55, No. 8, 1971, pp. 3624–3636.

[19]Crawley, D. J., Tolmie, E. D., and Huntress, A. D., "Evaluation of a New Silicone Fluid for Diffusion Pumps," *Transactions of the 9th National Vacuum Symposium,* Macmillan, New York, 1962, pp. 399–403.

[20]Huntress, A. D., Smith, A. L., Power, B. D., and Dennis, N. T. M., "A New Silicone Diffusion Pump Fluid," *Transactions of the 4th National Vacuum Symposium,* Pergamon Press, New York, 1958, pp. 104–111.

[21]Petraitis, D. J., Private communication, McGhan Nusil Corp., Carpinteria, CA, June 1986.

[22]Shapiro, H., and Hanyok, J., "Monomolecular Contamination of Optical Surfaces," *Vacuum,* Vol. 18, No. 11, 1968, pp. 587–592.

[23]Glassford, A. P. M., "The Response of a QCM to a Liquid Deposit," *Journal of Vacuum Science and Technology,* Vol. 15, No. 16, 1978, pp. 1836–1843.